Kinetics of ion-induced transformations in β-NiAl thin films as characterized by *in situ* electrical resistivity measurements

R. M. N. Miranda,* M. A. Z. Vasconcellos, and M. N. Baibich
Instituto de Física, Universidade Federal do Rio Grande do Sul, 91501-970, Porto Alegre, RS, Brazil

J. A. T. Borges da Costa†
Departamento de Física, Universidade Federal de Santa Maria, 97105-900, Santa Maria, RS, Brazil
(Received 11 July 1997; revised manuscript received 9 March 1998)

In situ electrical resistivity of thin film β-NiAl at 77 K under 120 keV Ar^+ irradiation has been measured as a function of the total dose for film thickness of 25, 37.5, 50, 62.5, and 75 nm. A qualitative change was observed in the resistivity versus dose behavior for 50 nm films that cannot be explained by the standard kinetic models. It is shown that depth-dependent cross sections account for the phenomenon as well as for the variety of dose-dependent electrical behaviors reported in the literature. [S0163-1829(98)06129-3]

I. INTRODUCTION

Electrical resistivity measurements have been extensively used to follow structural transformations in solids due to a variety of physical processes, such as thermal treatments or pressure effects. Damage from ion irradiation of materials has been studied using *in situ* electrical resistivity measurements rather frequently over recent years. In a previous work[1] the dose dependence of the *in situ* electrical resistivity of a 50 nm β-NiAl film under 120 keV Ar^+ irradiation at 77 K was reported. The results were interpreted according to simple composite models assuming that local transformations of the solid by successive ion impacts produce different conduction phases. The observed maximum in the resistivity was explained as a result of a competition between two such phases: a higher resistivity phase is dominant at low doses and a lower resistivity phase determines the high dose behavior.

In the conclusions of Ref. 1 it was pointed out that, besides no amorphization having been observed, the values obtained for the cross-sectional areas of the ion-induced transformations differed from the amorphization cross section of 120 keV Ar^+ ions hitting a 72 nm NiAl film at 77 K reported by Jaouen and co-workers.[2] These differences were attributed to either the presence of preexisting defects in the film produced by ion mixing in Ref. 2 (different sample preparation conditions are expected to explain different phase evolutions) or to a greater probability of inducing transformation in a NiAl film at depths between 50 and 72 nm by 120 keV Ar^+ ions.

In order to test the latter hypothesis, which can be more generally fomulated as a depth dependence of the probability of an energetic ion to induce resistivity changes in a solid, in the present work a series of samples of thin film β-NiAl has been prepared with varying thickness and submitted to the same irradiation conditions as those of Ref. 1. The *in situ* electrical resistivities of those samples have been measured and the results are here interpreted according to simple kinetic models that have been extended[3] to include film thickness effects through variable cross sections for ion-induced transformations.

Differently to what has been suggested in Ref. 1, here we conclude that the probability of inducing transformation in a NiAl film at depths between 50 and 77 nm is not greater than at depths down to 50 nm. In fact, we have found a maximum for one of the transformation cross sections at depths between 37.5 and 50 nm. However, the idea that depth dependence of ion-induced transformation can account for the phenomenology has proven to be valid.

II. PHENOMENOLOGY

Early models on the dose dependence of ion irradiation effects[4] assumed that each incident ion produces a homogeneous transformation inside an effective cylinder drawn around the projected track in the direction of incidence. In certain cases, a better fitting to the experimental data is obtained assuming that the same region of the material must cumulate the effects of two or more incident ions in order to induce transformations.

An important improvement to this approach was proposed by Carter and Webb,[5] who extended a previous model by Dennis and Hale.[6] While studying ion-beam-induced amorphization of silicon, these authors assigned some sort of structure to the tracks of energetic ions impinging the surface of crystalline silicon by assuming that each ion creates simultaneously amorphous and disordered regions. However, it is important to notice that modeling in terms of cross-sectional areas of effective cylinders implicitly disregards any depth dependence of the radiation-induced effects. Although this type of dependence has been studied both experimentally[7] and theoretically[8] for atomic mixing, to our knowledge it has not yet been explicitly taken into account in the study of structural transformations.

Due to the finite range of energetic ions in matter, one expects different damage and excitation levels at different depths from the irradiated surface, a subject that has been extensively studied for decades.[9,10] In fact, as earlier pointed out by Dennis and Hale,[6] cross-sectional areas for specific transformations must be understood as average values. They are physically meaningful as long as the energy distribution function for relevant damage and excitation processes is flat

over the entire layer under investigation. This condition is fulfilled, at least approximately, by most experiments on thin-film modification by high-energy heavy-ion irradiation reported in the literature.

In spite of the success of the above-mentioned models, some deviations from their predicted dose dependence behavior are found in independent work, especially in the high-dose limit. These deviations can be seen in the published resistivity versus dose plots of (i) 70 nm $Fe_{60}Co_{40}$ films irradiated at 77 K by different ions reported by Rivière *et al.*;[11] (ii) 40 nm $AuIn_2$ films irradiated at 125 K by 300 keV Ar^+ ions reported by Miehle and co-workers;[12] and (iii) β-NiAl films of various thickness irradiated at 77 K by 120 keV Ar^+ ions reported in the present work. In (i) a small but sudden additional increase in the resistivity (a ''knee'') occurs at doses between 0.4 and 0.5 dpa of 60 keV Ne ions and a minimum after a maximum in the resistivity occurs at doses between 0.1 and 0.2 dpa that is followed by a maximum at higher doses of 140 keV Ar^+ ions. In (ii) a knee is also found that is qualitatively the same as that described in (i) but quantitatively much larger at doses slightly above 0.5 dpa of 300 keV Ar^+ ions.

Although small in some cases, these effects can only be included in the framework of a phenomenological approach by introducing a new hypothesis on the ion-induced transformations. Thermally activated mechanisms are neglected since we are considering only low-temperature and low current experiments. As we shall see in the following, the qualitative differences can be explained in terms of the depth dependence of the cross sections for the ion-induced transformations.

III. EXPERIMENTS

Thin-film samples were made by sequential electron-gun evaporation of bilayers of Ni and Al following the scheme $[\mathrm{Al}(7.5\ \mathrm{nm})/\mathrm{Ni}(5\ \mathrm{nm})]_n$, where $n=(2,3,4,5,6)$, producing samples with a final thickness of 25, 37.5, 50, 62.5, and 75 nm, respectively. The samples were grown at rates of 0.2–0.6 nm/s and base pressures of 10^{-6} mbar inside the chamber. Films were deposited over an oxidized Si substrate using a mask to obtain a four-probe geometry suited for resistivity measurements. As-deposited multilayers were annealed under high vacuum at 773 K over 2 h in order to produce the homogeneous β-NiAl alloy, as identified by post-treatment x-ray-diffraction measurements.

Ion irradiation experiments were performed with 120 keV of Ar^+ and 300 keV of Xe^+ with fluences up to 2.5×10^{15} ions/cm^2. The ion current density was low enough ($\leqslant 100$ nA/cm^2) to avoid sample heating. The irradiation energies were determined from TRIM-95 (Ref. 9) simulations, such that calculated maxima of the energy and vacancy deposition profiles occurred at the middle of the sample of the largest thickness.

All samples were characterized before and after irradiation by Rutherford backscattering (RBS) and x-ray diffraction at room temperature. RBS spectra were obtained by irradiation with a 760 keV He^{++} beam at normal incidence and a detection angle of 165°. X-ray-diffraction spectra were obtained using a $\Theta/2\Theta$ geometry with a Cu source. The sample holder was allowed to spin in the sample plane during the measurements in order to minimize texture effects.

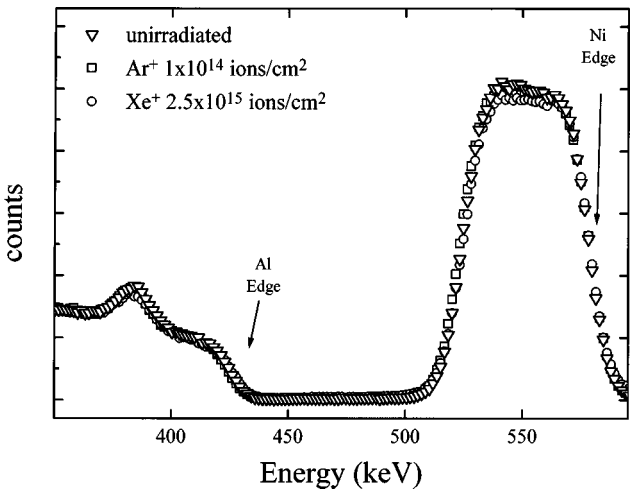

FIG. 1. Rutherford backscattering spectra of 50 nm films of β-NiAl deposited over oxidized Si substrates and irradiated with 1×10^{14} Ar^+ at 120 keV and with 2.5×10^{15} Xe^+ at 300 keV.

The modifications induced by Ar^+ irradiation on the samples were continuously monitored using *in situ* electrical resistivity measurements.[13] A liquid-nitrogen refrigerated sample holder for low-temperature irradiation and *in situ* electrical resistivity measurements system was built. The sample holder supports up to 24 samples in four positions (six samples/position). Substrate temperatures were maintained at 77 K during irradiation. Resistivity measurements were recorded *in situ* as a function of the total ion dose using a homemade system based on synchronous detection technology.[14] For the electrical contact between wires and film surfaces, an appropriate conductive low-temperature resin was used. The electrical current for resistivity measurements was 0.2 mA, guaranteeing the overall resolution of ≈ 50 ppm for resistivity changes. The automated data acquisition system allowed the measurement of up to nine experimental points per second. An aluminum mask was mounted in front of the films in order to allow irradiation in a controlled area and also to avoid irradiation of the contacts.

Figure 1 compares the RBS spectra of different samples of 50 nm-thick β-NiAl films that have been irradiated to different total doses of Ar^+ and Xe^+ ions. The portion of the spectra that represents the interface between the β-NiAl film and the SiO_2 substrate shows no broadening of the signal of each element, thus indicating that the irradiations do not induce any detectable interdiffusion between film and substrate. The same has been observed for all the film thickness in this work.

Figure 2 shows spectra obtained from x-ray-diffraction measurements for unirradiated and irradiated samples of β-NiAl film with 50 nm thickness. The Si substrate is identified by the lines (111), (222), and (511). Lines labeled (100) and (110) correspond to the β-NiAl phase. As can be seen, no evidence of crystalline to amorphous transformation is observed, independent of the dose. In performing a detailed scan over the main peaks for β-NiAl phase and determining the peak position relative to a standard (Silicon), the only modification observed is a shift in the peak position that is associated to small changes in the lattice parameter.[15]

Figure 3 shows the results of the electrical resistivity mea-

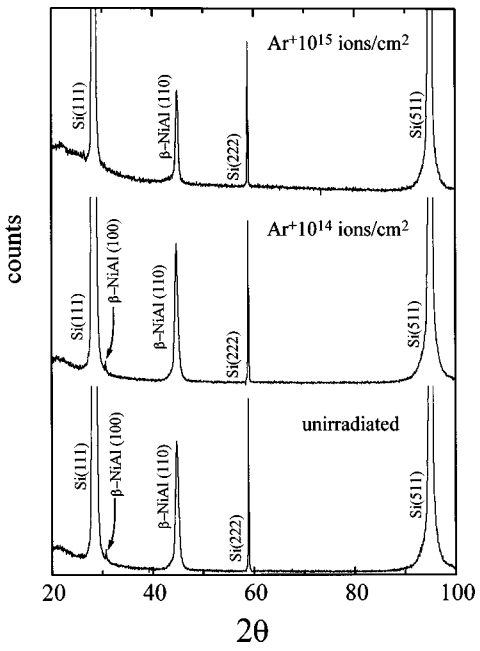

FIG. 2. X-ray-diffraction spectra of 50 nm films of β-NiAl deposited over oxidized Si substrates and irradiated to different doses of 120 keV Ar^+ ions.

surements at substrate temperatures of 77 K, presented as plots of the changes in electrical resistivity $\Delta\rho$, normalized by its initial value ρ_o, versus the total dose, ϕ. These plots show the same qualitative behavior for samples with thickness of 25, 37.5, 62.5, and 75 nm, namely, the rate of change of the electrical resistivity is high in the beginning of the implantation and, next, for doses higher than about 1×10^{14} Ar^+/cm^2, the relative variation in electrical resistivity $\Delta\rho/\rho_o$ increases at a lower rate, resulting in a saturation-like behavior. For the samples with thickness of 50 nm a qualitatively different behavior is observed. For these samples a maximum in $\Delta\rho/\rho_o$ occurs at doses of about 5×10^{13} Ar^+/cm^2. This is followed by a pronounced decrease in the electrical resistivity up to doses of about 2×10^{14} Ar^+/cm^2, where a broad minimum is reached. After that, $\Delta\rho/\rho_o$ increases for increasing doses at a very slow rate. This latter behavior is similar to what has already been described in the literature for other systems,[2,11] as discussed in Sec. II.

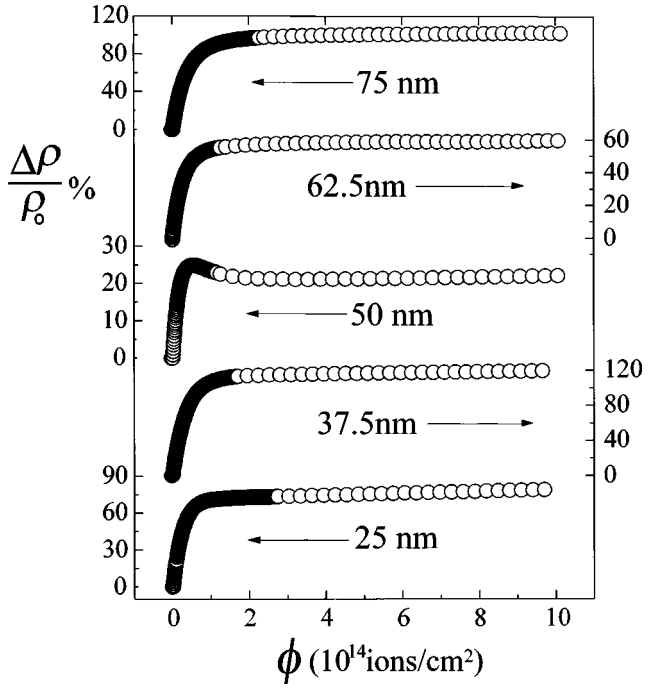

FIG. 3. Relative changes in electrical resistivity normalized by its initial value ($\Delta\rho/\rho_o$) as a function of the total Ar^+ dose (ϕ) for samples with thickness of 25, 37.5, 50, 62.5, and 75 nm.

It is worth it to notice at this point how the largest value of $\Delta\rho/\rho_o$ in the dose range of our measurements changes with film thickness. For the thinner films it increases, then, for the 50 nm film it decreases, and, finally, for the thicker films, it again increases. From this observation, one is lead to conclude that a transformation occurs between 37.5 and 50 nm that lowers the total resistivity of the 50 nm films.

It is a common practice to relate variations of sample electrical conduction properties to the fraction of transformed material. In Ref. 1, a linear relation was assumed between the measured conductivity σ_m, and the volume fractions of the film x_k, transformed to states of different electrical resistivities σ_k, that reads

$$\sigma_m(\phi)=\sum_k x_k(\phi)\sigma_k, \tag{1}$$

where the dose dependence is indicated. Equation (1) can be shown to be an approximation of Landauer's expression[16] for the conductivity of a composite material, when the conductivities of its components are similar, and, on the other hand, it is an exact expression for a multilayered structure. In any case, it is to be taken as a first-order approximation of the general case. As applied to our experimental results, this expression must be understood as valid due to the lamellar structure resulting from depth-dependent transformations. Lamellar conduction is here assumed from the moment that, at a certain depth, the ion transformed regions percolate. In a computer simulation using the parameters found in this work, the limit for percolation of a system composed of transformed environments (for random deposition of ions) is found as 3.1×10^{13} ions/cm^2, which is below any of the observed effects treated in this work.

For a system consisting of two phases, i.e., assuming that only one new phase is formed under ion irradiation, the volume fraction of the transformed material, $x(\phi)$, can be obtained from Eq. (1) as

$$x(\phi)=\frac{\sigma_m(\phi)-\sigma_o}{\sigma_f-\sigma_o}, \tag{2}$$

where σ_o and σ_f are the initial and final conductivities of the film, respectively.

Through Eqs. (1) and (2), it is possible to study the transformation kinetics of ion irradiated solids by following changes in electrical conduction properties. After converting the electrical conductivity raw data to concentrations, one needs to compare different kinetic regimes. This has been accomplished[2] through the kinetic equation

$$x(\phi)=1-e^{-a\phi^n}, \tag{3}$$

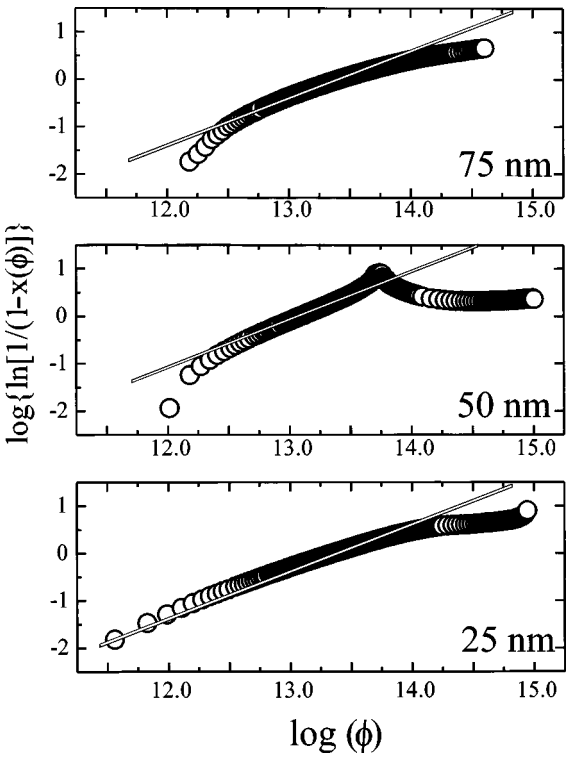

FIG. 4. *In situ* electrical resistivity raw data plotted according to Eq. (4) for samples irradiated with Ar^+ and with thickness 25, 50, and 75 nm. The straight lines are the best fits to the Gibbons' model.

where a and n are constants. In fact, this can be viewed as an adaptation of the expression $x(t)=1-e^{-at^n}$, used to study phase transformation kinetics in metals and alloys.[17] For low-temperature ion-induced transformations the time t has been replaced by the dose ϕ.

Taking the reciprocal of $1-x(\phi)$ from Eq. (3) and calculating the ln and log of the resulting expression, one obtains

$$\log\left[\ln\left(\frac{1}{1-x(\phi)}\right)\right]=\log a+n\ \log\ \phi. \tag{4}$$

According to Eq. (4), a plot of $\log(\ln\{1/[1-x(\phi)]\})$ vs $\log(\phi)$ (Avrami's plot) is a straight line of slope n in all dose ranges. If the slope of the line fitted to experimental data changes, then different transformation mechanisms dominate in each dose range. In particular, if $n=1$ then a Gibbons' picture holds.

Gibbons' model[4] (originally conceived to describe amorphization of crystalline silicon under heavy-ion irradiation) has been largely employed to analyze transformation kinetics of irradiated solids. In its simplest version, it assumes the coexistence of two phases during irradiation. Transformation from one phase to the other is assumed to occur homogeneously inside a cylinder of sectional area $a=A_i$, drawn around each ion trajectory.

Figure 4 shows the experimental results of the present work plotted according to Eq. (4) for samples irradiated with Ar^+ and with thickness 25, 50, and 75 nm. The straight lines represent the best fits of Gibbons' model to our data. In all cases, a good fit is obtained only in a limited dose range. For the fluxes employed in the present work ($\dot{\phi}\leqslant 100$ nA), this dose range corresponds to the transformations occurring in the first few seconds of the experiment. For the 50 nm samples, a negative slope would be obtained by fitting a straight line in the dose range from about 5×10^{13} to about 1×10^{14} Ar^+/cm^2. Hence, the beginning of this dose range must be interpreted as the onset of the consumption of the new phase, since the signal of the derivative of the left-hand side of Eq. (4) is equal to the signal of $dx(\phi)/d\phi$. In the following sections it is shown why this consumption does not seem to occur for samples of different thickness.

IV. THEORY

There are at least two simple ways to explain the whole family of resistivity versus dose curves reported during the past few years. In the first, one adds more and more conduction phases, and corresponding transformation rules, to the previous models. This alternative seems too artificial if not supported by further experimental evidence. In the second, one assumes that the same conduction phases occur in the whole sample with a nonuniform depth distribution resulting from a varying transformation probability measured by depth-dependent cross sections. This latter description is supported by what is well known about the stopping of ions in matter, namely, that the cross sections for different damage and excitation processes depend on ion mass and energy.[9,10] As an ion penetrates a solid, it loses its energy in these processes and the cross sections for the succeeding transformations change. Therefore, a depth dependence of damage and excitation levels is expected. This produces a layered structure undergoing transformation at different rates. Depending on the electrical conduction properties of these layers, their parallel association gives rise to sequences of knees and/or maxima in the resistivity versus dose plots, as shall be shown in the following.

As in the previous work,[1] it is here assumed that the consumption of the first phase formed by ion irradiation, as suggested by Fig. 4, is accompanied by the formation of another phase of lower resistivity. Three conduction phases thus contribute to the total conductivity of the irradiated samples. The maximum in the resistivity of the 50 nm samples is then described as the result of a competition between the two phases produced by ion irradiation, namely, the higher resistivity state that dominates the electrical behavior of the samples in the low-dose range and the lower resistivity state that dominates the high-dose range and is responsible for the consumption of the former.

In order to include depth-dependent effects, let z to be the direction of ion incidence that is perpendicular to the free surface of the solid. Let the portion of the film between positions z_{i-1} and z_i, measured from its free surface be its ith slice taken parallel to its surface, as shown in Fig. 5. Next, a model is introduced to describe the transformation kinetics in the slices, with slice-dependent cross sections.

In the present work, two models have been selected that qualitatively explain our experimental observations. In what follows, it is suggested that quantitative differences allow us to conclude about the relative validity of their hypothesis. The first is the three phase Gibbons' model,[4] modified to include a depth dependence of the ion-induced transformations, according to which the solid transforms locally to dif-

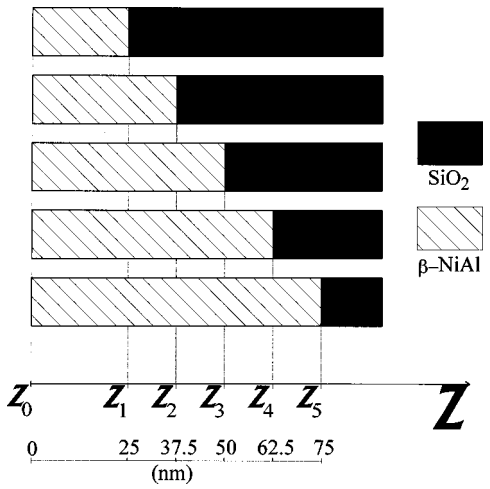

FIG. 5. Schematic diagram of the slicing adopted for the fitting procedure described in Sec. V.

ferent states due to the effects of 0, 1, and 2 or more ion impacts over the same region. Before irradiation, the whole solid is in a state of resistivity ρ_o. After the first ion impact, a region of cross section A_i transforms to a state of resistivity ρ_1, i.e., $A_i \cap o = 1$. When the effects of a second impact overlap this new phase, it transforms to a state of resistivity ρ_2, i.e., $A_i \cap 1 = 2$. Further impacts do not change the sate of this latter phase, i.e., $A_i \cap 2 = 2$. In order to fit the electrical behavior of the 50 nm samples, $\rho_o < \rho_2 < \rho_1$, i.e., the solid transforms to a higher resistivity state after the first ion impact and to a lower resistivity state from the second impact on. The latter, permanent, phase is formed by the consumption of the former, transient, one. If this model is adopted, the volume fractions $x_{k,i}$ of the conduction phases $k = o,1$, and 2, change with dose ϕ in the ith slice, according to the equations

$$\frac{dx_{o,i}}{d\phi} = -A_i(z_i)x_o, \tag{5}$$

$$\frac{dx_{1,i}}{d\phi} = A_i(z_i)[x_o - x_1], \tag{6}$$

$$\frac{dx_{2,i}}{d\phi} = A_i(z_i)x_1, \tag{7}$$

where $A_i(z_i)$ is the transformation cross section in the slice ending at z_i.

Solving the set of Eqs. (5)–(7) results in

$$x_{o,i}(\phi) = e^{-A_i(z_i)\phi}, \tag{8}$$

$$x_{1,i}(\phi) = A_i(z_i)\phi e^{-A_i(z_i),\phi}, \tag{9}$$

$$x_{2,i}(\phi) = 1 - [1 + A_i(z_i)\phi]e^{-A_i(z_i)\phi}. \tag{10}$$

The second model considered in this work is the simplified model proposed in Ref. 1. This model assumes that every ion impact produces simultaneously local transformations from the initial state of resistivity ρ_o to a transient state of higher resistivity ρ_H and to a permanent state of lower resistivity ρ_L, i.e., $\rho_o < \rho_L < \rho_H$. The cross sections of the transformations leading to these states in the slice ending at z_i are denoted by $A_k(z_i)$, where $k = o,H,L$. Overlapping a region of the solid in state k by the effects of subsequent impacts, induces transformation according to the following rules: $A_H \cap o = H$; $A_L \cap o = L$; $A_H \cap H = H$; $A_L \cap H = L$; $A_H \cap L = L$ and $A_L \cap L = L$. Accordingly, the kinetic equations that give the rates of change of the volume fractions, in the ith slice, having undergone transformation to each of these states, are

$$\frac{dx_{o,i}}{d\phi} = -[A_H(z_i) + A_L(z_i)]x_o, \tag{11}$$

$$\frac{dx_{H,i}}{d\phi} = A_H(z_i)x_o - A_L(z_i)x_H, \tag{12}$$

$$\frac{dx_{L,i}}{d\phi} = A_L(z_i)[x_o + x_H]. \tag{13}$$

Solving Eqs. (11)–(13) for the slice ending at z_i, it is found that the volume fractions of the phases labeled o (unirradiated), H, and L are given by

$$x_{o,i}(\phi) = e^{-[A_H(z_i) + A_L(z_i)]\phi}, \tag{14}$$

$$x_{H,i}(\phi) = e^{-A_L(z_i)\phi} - e^{-[A_H(z_i) + A_L(z_i)]\phi}, \tag{15}$$

$$x_{L,i}(\phi) = 1 - e^{-A_L(z_i)\phi}. \tag{16}$$

In both models, the state o represents the unirradiated surface and the transformation rules lead assymptotically to the low resistivity state. The transformation rules $A_2 \cap 1 = 2$, of the first model, and $A_L \cap H = L$ of the second model, are suggested by independent experimental observation of reordering after disordering by particle irradiation of the NiAl system.[18] The main difference between the two models is that while in the former the low resistivity state can only be produced by some ''reordering'' of the high resistivity state, in the latter this state can also be produced by the first ion impact over the unirradiated surface.

The next step is to relate the fractions of transformed material to variations of electrical conduction properties. It is again assumed that the mean electrical conductivities of the above mixtures of phases can be calculated by Eq. (1). Under the above hypothesis the global conductivity of the film σ_m can be calculated by first substituting the $x_{k,i}(\phi)$'s into Eq. (1) to obtain the mean conductivities of the slices $\sigma_{m,i}$, and then making a parallel association of the slices through

$$\sigma_m = \sum_{i=1}^{N} \ell_i \sigma_{m,i}, \tag{17}$$

where $\ell_i = (z_i - z_{i-1})/\ell$ is the thickness of the ith slice relative to the total thickness of the film ℓ, and N is the number of slices. The layered symmetry of the problem suggests that Eq. (1) is a good approximation to the exact value of the global conductivity.

According to the above, if the three phases Gibbons' model described by Eqs. (5)–(7) is adopted, the conductivity of the film is given by

$$\sigma_m(\phi)=\sigma_2+\sum_{i=1}^{N} \ell_i[(\sigma_o-\sigma_2)-(\sigma_2-\sigma_1)A_i\phi]e^{-A_i\phi}. \tag{18}$$

If the model described by Eqs. (11)–(13) is adopted, then

$$\sigma_m(\phi)=\sigma_L+\sum_{i=1}^{N} \ell_i[(\sigma_H-\sigma_L)e^{-A_L(z_i)\phi} + (\sigma_o-\sigma_H)e^{-[A_H(z_i)+A_L(z_i)]\phi}]. \tag{19}$$

Of course, the cross-sectional areas appearing in the above equations must be interpreted as average values over the corresponding slices. Equations (18) and (19), and all those that can be analogously obtained by adopting other kinetic models, are suitable to study depth-dependent effects of the modification of materials by ion beams. This is carried out by fitting these kinetic equations to resistivity versus dose measurements.

V. ANALYSIS

In this section, the experimental results from the *in situ* measurements of electrical resistivity as a function of the irradiation dose are analyzed on the basis of the two models presented in the previous section by fitting Eqs. (18) and (19). The fitting parameters are σ_1, σ_2, and $A_i(z_i)$ for the first model, and σ_H, σ_L, and $A_k(z_i)$ for the second. These are constrained to satisfy the relations $\sigma_1,\sigma_2,A_i(z_i)>0$ and $\sigma_o>\sigma_2>\sigma_1$; $\sigma_H,\sigma_L,A_k(z_i)>0$ and $\sigma_o>\sigma_L>\sigma_H$. Besides, the values of $\sigma_m(\phi)$, σ_o and ℓ_i are determined experimentally. The fitting software used in the present work[19] applies the Levenberg-Marquardt nonlinear least-squares method.[20,21]

For a set of films of variable thickness, under the same irradiation conditions, the physical processes occurring in the thinnest film are assumed to be the same occurring in the most superficial slice (of the same thickness of the thinnest film) of the other thicker films. Referring to Fig. 5, the transformations occurring in the film with total thickness z_1-z_0 are the same occurring in the slice ending at z_1 of films with thickness z_2-z_0, z_3-z_0, etc. Under this assumption, the data from the thinnest film are fitted to Eqs. (18) and (19) considering only terms on z_1 and making $\ell_1=1$, since $\ell_1=(z_1-z_0)/\ell$, where $\ell=z_1-z_0=25$ nm. By this process, the values of $A_k(z_1)$ and $\sigma_{k\neq o}$ are determined. Then, the data from the next thicker film ($\ell=z_2-z_0=37.5$ nm) are fitted to the same equations considering terms up to z_2, i.e., the film is considered as formed by two slices of relative thickness $\ell_1=(z_1-z_0)/\ell=25/37.5\simeq 0.67$ and $\ell_2=(z_2-z_1)/\ell=12.5/37.5\simeq 0.33$. According to our assumptions, the fitting parameters of the top slice are known from the study of the thinnest film and, therefore, only the values of the $A_k(37.5$ nm) need, in principle, be determined. The fitting proceeds by including further and further slices in the analysis as the film grows thicker. The relative slice thickness of the other films are $\ell_1=0.50$ and $\ell_2=\ell_3=0.25$ for the 50 nm film; $\ell_1=0.40$ and $\ell_2=\ell_3=\ell_4=0.20$ for the 62.5 nm film, and $\ell_1\simeq 0.33$ and $\ell_2=\ell_3=\ell_4=\ell_5\simeq 0.17$ for the 75 nm film.

The above fitting procedure cannot be strictly followed because, due to substrate and free-surface influences, the top layer of a thick film has not exactly the same properties of a thin film with the same thickness. In particular, the values of σ_o are different for films with different thickness. Figure 6 shows an almost linear decrease of the initial values of the resistivity ρ_o with film thickness, ℓ. The conductivities of the phases formed by irradiation must, therefore, be calculated at each fitting step.

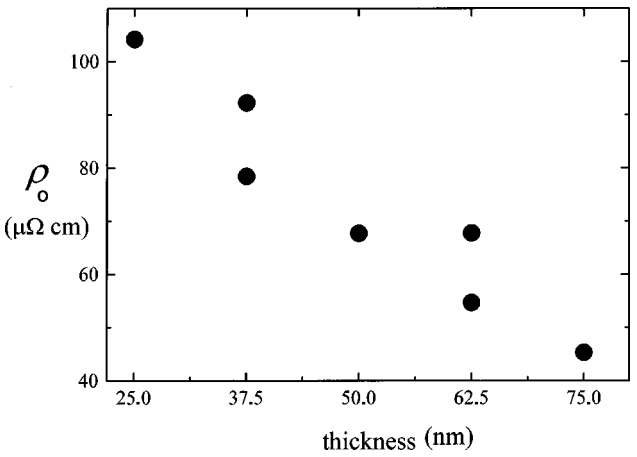

FIG. 6. Initial electrical resistivity ρ_o measured at 77 K for samples with different thickness, ℓ.

Both Eqs. (18) and (19) fit quite well our experimental results for samples with a thickness of 25, 37.5, 62.5, and 75 nm. Figure 7 compares the fittings of both equations to our raw data from a 50 nm sample. As it is readily seen, only Eq. (19) fits our results in the dose range around the maximum.

Figure 8 shows the values of ρ_H and ρ_L, obtained from the corresponding fitting parameters σ_H and σ_L, normalized to the initial value of the resistivity for each film thickness $\rho_o(\ell)$, plotted against ℓ. The oscillations in ρ_H/ρ_o and ρ_L/ρ_o are within the errors and, therefore, these values can

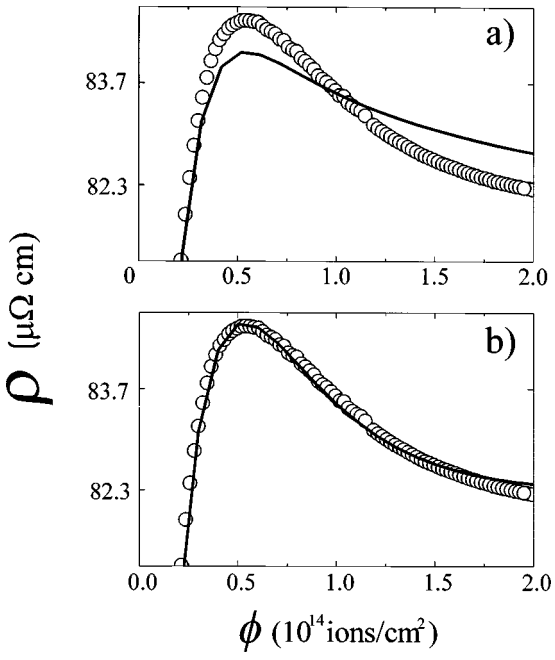

FIG. 7. Comparison of the fittings (solid lines) of both Eqs. (18) (7.a) and (19) (7.b) to our raw data (open circles).

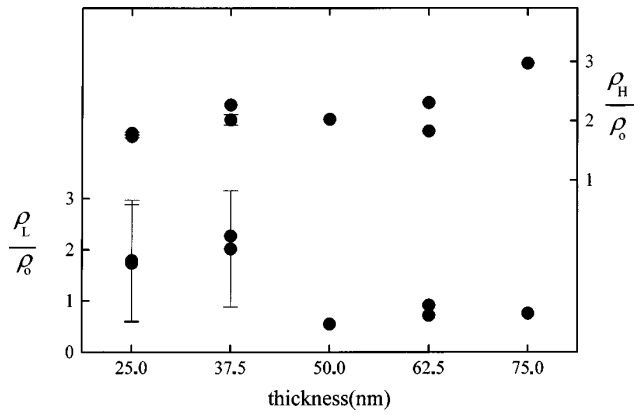

FIG. 8. Electrical resistivities of the phases labeled H and L obtained from the fittings of Eq. (19) and normalized to ρ_o for samples with different thickness.

be considered nearly constant, i.e., they represent well-defined conduction phases. This observation consistently reinforces the hypothesis of the formation of two new phases.

The fitted cross-sectional areas $A_H(z_i)$ and $A_L(z_i)$, for the transient and permanent phases, respectively, are plotted against z_i in Figure 9. A sudden decrease in A_H occurs between 37.5 and 50 nm, while A_L shows a maximum at this layer and is almost zero for all other layers.

VI. CONCLUSIONS

Under the experimental conditions of the present work (low temperature and low current), the transformations induced by each ion impact are restricted to the volume of its atomic collision cascade, and the probability of overlapping the same region of the film by two *simultaneous* cascade events is very low. Therefore, transformation of film properties can be described as a result of the cumulative effect of the space overlapping of *independent* cascade events. This is the basic assumption of the models presented in Sec. IV.

In Ref. 1 we have employed these two models without depth dependence of the cross sections and, then, it was not possible, on the basis of the quality of the fittings, to determine which mechanism is operating in this system. Here they produce quantitatively different behaviors, as shown in Fig. 7. The inclusion of depth dependence of transformations constrains the values of the conductivities in order to fit the results of all other thickness, thus making a harder fitting to data from 50 nm films. This result suggests that the second is the mechanism that better accounts for all observations and, therefore, the one that is more likely the actual sequence of events occurring in the irradiated films.

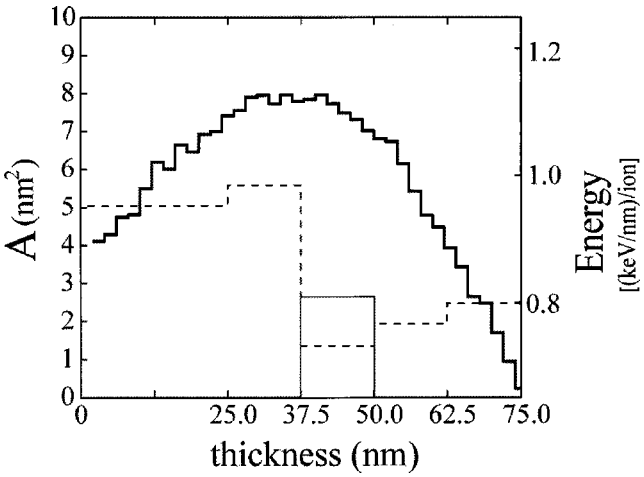

FIG. 9. Cross-sectional areas A_H (dashed line) and A_L (thin solid line) obtained from the fittings of Eq. (19) for samples with different thickness and energy deposition according to a TRIM-95 simulation (thick solid line).

In the framework of the present approach, the qualitatively different resistivity versus dose curves, observed for films of different thickness of the same material under the same irradiation conditions, are a result of different relative contributions of layers transforming to different states of electrical conductivity (to which we have refered as phases), to the total electrical resistivity of the film.

According to our x-ray-diffraction results,[15] the peak positions of the β-NiAl phase are shifted as irradiation doses are modified. These results are indicative of changes in the lattice parameter, which translates into changes in the resistivity, as this property is intimately connected to the structure and its changes.

The monotonical increase in resistivity towards saturation for the thinnest films may indicate an ion-target interaction process inducing disorder in the shallower layers of β-NiAl under 120 keV Ar^+ irradiation at 77 K. This is expressed as a high probability of transformation to a higher resistivity state, i.e., a large A_H for the slices ending at $z_i = 25$ nm and $z_i = 37.5$ nm, as shown in Fig. 9.

For the 50 nm films, the decrease in resistivity after the maximum at about 5×10^{13} Ar^+/cm^2 may be attributed to reordering by dense cascade processes between $z_i = 37.5$ nm and $z_i = 50$ nm. According to TRIM-95 simulations, the energy deposition has its maximum at this depth, which corresponds to about 80% of the projected ion ranges. This is expressed as a high probability of transformation to a state of resistivity ρ_L, i.e., a large A_L for the slice ending at $z_i = 50$ nm, as shown in Fig. 9. The contribution of this slice dominates the overall electric behavior of the film in the high-dose range. For low doses, the shallower layers quickly complete their transformation to the state of resistivity ρ_H, increasing the film resistivity.

One possible different physical mechanism leading to resistivity variations as well in region H as in region L might be related to a model for phase nucleation in metallic binary alloys put forward by Ossi.[22,23] According to this atomistic model, compositional changes occur at the interface between the collision cascades and crystal matrix during the final stages of the cascade so that the interface is enriched in one of the alloy components that captures one electron from the other component. Thus the former central region of the cascade is surrounded by a segregated shell. The appearence of such a modified region must be acompanied by changes in the lattice parameter as well as in the resistivity, as we have observed in our work.

If the above model accounts for the effects of the first ion impact over the unirradiated surface then, in order to fit the resistivity variations, our kinetic study shows that (a) no segregation should occur when the cascade-matrix interface overlapped a region where segregation was induced by a

previous ion impact ($A_H \cap H = H$); (b) the region overlapped by a dense cascade core (more likely to occur at depths where the energy deposition by the ion beam is maximum) should transform directly to a homogeneous state irrespective of its inital state ($A_L \cap o = L$, $A_L \cap L = L$ and $A_L \cap H = L$); (c) no segregration should occur in the homogeneous region transformed by a previous cascade core ($A_H \cap L = L$).

The saturating behavior observed for the thicker films is a result of the contribution of the deeper layers to the total resistivity. As shown in Fig. 9, between $z_i = 50$ nm and $z_i = 75$ nm, A_H is larger than A_L, i.e., the probability to transform the film to a state of resistivity ρ_H is higher for the deeper layers, as suggested in Ref. 1. Also, in the 62.5 and 75 nm films, the slice ending at $z_i = 50$ nm contributes to decrease the resistivity but, then, its contribution is weighted in Eq. (19) by the factors $\ell_3 = 0.20$ and $\ell_3 \simeq 0.17$, respectively. These are less than the weighting factor of the same slice to the resistivity of the 50 nm film, namely, $\ell_3 = 0.25$, and, therefore, the contribution of this slice is not enough to produce a net decrease in the resistivity of the thicker films. In other words, a 0.05 variation in the relative thickness of that slice produces the observed qualitative change in the resistivity versus dose curves. In conclusion, the dose dependence of electrical resistivity is very sensitive to film thickness.

The depth dependence of ion-beam-induced transformations also explains the qualitatively different dose dependencies of electrical resistivity reported in independent works[11,12] that we have mentioned in Sec. II. By changing the ion mass and energy, the type, depth, and relative importance of the transformations change, resulting in a whole family of curves with knees and maxima that can be fitted either by Eqs. (18), (19), or others that can be analogously obtained for other sequences of transformations.

ACKNOWLEDGMENTS

This work was supported in part by the Fundação de Amparo à Pesquisa do Estado do Rio Grande do Sul (FAPERGS, Brazil), the Conselho Nacional de Desenvolvimento Científico e Tecnológico (CNPq, Brazil), the Financiadora de Estudos e Projetos (FINEP, Brazil), and the Programa de Apoio ao Desenvolvimento Científico e Tecnológico (PADCT, Brazil).

*Electronic address: miranda@if.ufrgs.br and web: www.if.ufrgs.br/~miranda

†Electronic address: bdacosta@super.ufsm.br

[1] J. A. T. Borges da Costa, M. A. Z. Vasconcellos, S. R. Teixeira, C. Scherer, and M. N. Baibich, Phys. Rev. B **45**, 9626 (1992).

[2] C. Jaouen, J. Delafond, and J. P. Rivière, J. Phys. F **17**, 335 (1987).

[3] J. A. T. Borges da Costa, Ph.D. Thesis, Universidade Federal do Rio Grande do Sul, 1992.

[4] J. F. Gibbons, Proc. IEEE **60**, 1062 (1972).

[5] G. Carter and R. Webb, Radiat. Eff. Lett. Sect. **43**, 19 (1979).

[6] J. R. Dennis and E. B. Hale, J. Appl. Phys. **49**, 1119 (1978).

[7] B. Y. Tsaur, S. Matteson, G. Chapman, Z. L. Liau, and M.-A. Nicolet, Appl. Phys. Lett. **35**, 825 (1979).

[8] R. Collins and J. J. Jimenez-Rodriguez, Radiat. Eff. Lett. Sect. **68**, 19 (1982).

[9] J. F. Ziegler, J. P. Biersack, and U. Littmark, *The Stopping and Range of Ions in Solids* (Pergamon, New York, 1985).

[10] K. B. Winterbon, P. Sigmund, and J. B. Sanders, Mat. Fys. Medd. K. Dan. Vidensk. Selsk. **37**, 1 (1970).

[11] J. P. Rivière, P. Bouligand, J. F. Dinhut, and J. Delafond, Radiat. Eff. Defects Solids **114**, 145 (1990).

[12] W. Miehle, A. Plewnia, and P. Ziemann, Nucl. Instrum. Methods Phys. Res. B **59/60**, 410 (1990).

[13] R. M. N. Miranda, M. Sc. thesis, Universidade Federal do Rio Grande do Sul, 1996.

[14] M. Fin and M. N. Baibich, Rev. Fis. Appl. Instrum. **4**, 290 (1989).

[15] R. M. N. Miranda, M. A. Z. Vasconcellos, M. N. Baibich, and J. A. T. Borges da Costa, Nucl. Instrum. Methods Phys. Res. B **127/128**, 132 (1997).

[16] R. J. Landauer, J. Appl. Phys. **23**, 779 (1952).

[17] J. W. Cristian, *The Theory of Transformations in Metals and Alloys*, 2nd. ed. (Pergamon, Oxford, 1985).

[18] L. Thome, C. Jaouen, J. P. Riviere, and J. Delafond, Nucl. Instrum. Methods Phys. Res. B **7/8**, 591 (1985).

[19] Microcal Origin, Version 4.00, Copyright © 1991–1995 Microcal Software Inc., Northhampton, MA, USA.

[20] K. Levenberg, Q. Appl. Math. **2**, 164 (1944).

[21] D. W. Marquardt, SIAM (Soc. Ind. Appl. Math.) J. Appl. Math. **11**, 431 (1963).

[22] P. M. Ossi, Mater. Res. Soc. Symp. Proc. **373**, 27 (1995).

[23] P. M. Ossi, Z. Phys. B **93**, 242 (1994).